The different organization of water in zeolite L and its MOF mimic

Ettore Fois*, Gloria Tabacchi*

Department of Science and High Technology and INSTM, Università degli Studi dell'Insubria, Via Valleggio 11, I-22100 Como, Italy

* corrisponding authors:
ettore.fois@uninsubria.it; gloria.tabacchi@uninsubria.it

Abstract.
Confinement of molecules inside one dimensional arrays of channel-shaped cavities has led to an impressive number of technologically interesting materials. However, the interactions governing the properties of the supramolecular aggregates still remain obscure, even in the case of the most common guest molecule: water. Herein, we use computational chemistry methods (#compchem) to study the water organization inside two different channel-type environments: zeolite L – a widely used matrix for inclusion of dye molecules, and ZLMOF – the closest metal-organic-framework mimic of zeolite L. In ZLMOF, the methyl groups of the ligands protrude inside the channels, creating nearly isolated nanocavities. These cavities host well-separated ring-shaped clusters of water molecules, dominated mainly by water-water hydrogen bonds. ZLMOF channels thus provide arrays of „isolated supramolecule" environments, which might be exploited for the individual confinement of small species with interesting optical or catalytic properties. In contrast, the one dimensional nanochannels of zeolite L contain a continuous supramolecular structure, governed by the water interactions with potassium cations and by water-water hydrogen bonds. Water molecules impart a significant energetic stabilization to both materials, which increases by increasing the water content in ZLMOF, while the opposite trend is observed in zeolite L. The water network in zeolite L contains an intriguing hyper-coordinated structure, where a water molecule is surrounded by 5 strong hydrogen bonds. Such a structure, here described for the first time in zeolites, can be considered as a water pre-dissociation complex and might explain the experimentally detected high proton activity in zeolite L nanochannels.

Introduction

An appealing way to control randomly oriented molecules is to use a confining matrix to impart a preferential orientation, which allows guest species to respond cooperatively to electro-optical stimulations [1]. This strategy

has produced materials of technological relevance based on the collective behaviour of organized molecular objects [23,4]. In optoelectronic devices, it is crucial that the individual molecular responses sum up in a fast and effective manner [5,6]. The incorporation of photoactive species in nanoporous matrices enhances the emission properties, as well as the catalytic and photocatalytic activity, [5,7–9] because strict confinement rules the aggregation of organic chromophores. Excitation energy transfer in artificial antenna systems[5], for example, has concrete applications in solar energy technology [9,10]. For these reasons, the realization of organized supramolecular systems in nanoporous frameworks is a steadily growing research area [9]. Zeolite cages have long been exploited to create confined nanostructures for optoelectronics [11], like metal clusters,[12–14] quantum dots,[10,15,16] or lanthanide complexes [17], and the practical applications of zeolite-based functional composites from effect pigments[18], to theranostic agents [19,20], keep on increasing in number and performances.

Zeolite confinement also leads to intriguing assemblies of very simple molecules. For example, hydrophobic silicalite hosts water nanostructures of rather small lenght, nicknamed ‘‘nanoworms“ [21–23], whereas straight, water chains are found in the one-dimensional channel systems of two narrow-pore zeolites: natural bikitaite [24–33] and synthetic Li-ABW[34–38]. Size, topology and chemical nature of the zeolite pores are responsible of the spectacular diversity of supramolecular systems exhibited by zeolitic water, ranging from spherical clusters in LTA cages [39–41],to triple helices in large-pore VFI [42–44].These confined water aggregates also explain the high resistance of zeolites to mechanical stress [45–47]. At very high pressure, the void-space architecture of zeolites can promote formation of complex arrangement of guest molecules [48], which act as „pillars“ preventing thus the pressure-induced collapse of the framework [49–54].

From a broader viewpoint, the study of the structural arrangement of water molecules in zeolite cages has greatly contributed to our knowledge of host-guest interactions [1,22,55] and to its application to zeolite L hybrid composites [56]. A deeper understanding would be key to realize new host-guest materials guided by atomistic-level design. Indeed, the insight gathered on zeolite-based hybrids has already fostered the extension of the idea to mesoporous silicas/organosilicas [7,57–60], [61,62], layered materials,[63–66] and metal organic frameworks (MOF) [1,3,67,68 69–71]. Yet such enormous field still remains little explored.

In contrast, the implementation of zeolite L hybrids (framework type: LTL)[72] has already accomplished practical application in strategic areas such as solar energy harvesting,[5,73–79] photonics,[80–82] and nano-medical technology.[19,83–85] The fabrication of confined architectures of chromophores for photon transport [5,9,57,86–88] and other light-operated systems[17,19,89] has made impressive progresses in the last few years. On the other hand, it is still to clarify how the microscopic interactions within the cages govern the peculiar behavior of guest species, and thus the commercially useful features of zeolite L devices. Computational approaches applied to zeolites [49,90–93], mesoporous silicas [3,94–96] and MOFs[97–99]) are increasingly popular be-

cause of the fundamental insight achievable through modeling. Theoretical studies elucidated the organization of several neutral dyes [79,100–103] and cationic chromophores[56,75,104–108] in zeolite L channels, along with their interaction with zeolitic framework, cations, and water. A detailed description of the channel entrances was also accomplished [109], thus attaining a molecular-level view of the interface processes governing the fabrication of these materials [110]. Combined with experiments, calculations have shown that dye-zeolite L composites can withstand GPa-pressures without alteration in the organization of the guests[111], which is important for extending the application of zeolite-based optical devices. Could it be possible to exploit such knowledge to favour the progress of MOF-based hybrid devices?

The self-assembly of metal ions as nodes and suitable ligands as spacers is a successful strategy to produce MOFs mimicking zeolite topologies [112,113], in spite of obvious differences in size of the cavities, chemical nature of the framework, and dimensions of the crystals. When combined with proper guests, MOFs they may form composites with exciting electro-optical properties[67]. MOFs having one-dimensional (1D) channel systems are particularly appealing for the fabrication of host-guest multifunctional hybrid materials [71 114].

A nice example is the "zeolite L-mimic metal–organic framework (ZLMOF)" built by Noh et al. from $[Ag_4Ni(L)_3]\cdot 3.5H_2O$ (L^{2-} = bis(methylthio)methylenepropanedioate), which features so-called "caterpillar-shape nanochannels"[115]. This ZLMOF represents to date the best structural mimic of zeolite L (ZL), as its channels have comparable shape and size. Specifically, both zeolite L and ZLMOF channels can be schematized by cylinders having, at normal conditions (298 K, 1 atm), a maximum internal diameter of 10.268 Å [116] and 11.970 Å [115], respectively. The free diameter of zeolite L channels (corresponding to the size of the channel opening) is 7.2 Å, while the free diameter of the ZLMOF channels is limited to 7.55 Å by the ligands' thiomethyl groups[115]. Both zeolite L and ZLMOF feature hexagonal arrays of channels, running along the *c*-axis; moreover, for both as-prepared materials, the channels contain clusters of water molecules [115,116].

In spite of the close structural similarity, the channels differ significantly in their hydrophobicity/hydrophilicity properties: while LTL is hydrophylic due to Al framework cations (Si/Al ratio =3) and K^+ ions in the pores, ZLMOF is partially hydrophobic owing to the thiomethyl groups protruding into its channel. On this basis, we expect that water molecules should have different interactions when confined in these materials, and therefore different supramolecular arrangements.

Herein we explore, with dispersion-corrected density functional theory (DFT), the structural organization of water molecules in as-prepared Zeolite L and ZLMOF, with the aim of attaining an atomistic-level understanding of the host-water and water-water interactions in the two materials. The amounts of water considered for ZLMOF and zeolite L correspond to those experimentally determined at

equal pressure –namely, 1 atm. The study of the arrangement of water molecules in the cavities could help to assess if water plays a significant role in the stability of this ZLMOF, and whether this framework might be possibly exploited as a nanocontainer of other species.What is the role played by the guest $(H_2O)_n$ clusters in the ZLMOF formation process? On the basis of crystallographic data, Noh et al. hypothesized that the water clusters could act as templates for the building of "caterpillar-shape-channels" [115]. This reasonable argument recalls the water-cation template effect proposed by Barrer for zeolite minerals[117], yet it does not describe the molecular-level interactions, nor does it explain how water may impart stabilization to the host-guest system. Understanding how water molecules are organized in the channels of ZLMOF, how their arrangements differs from water in zeolite L, and why these assemblies are stable, could deliver important insight on this unique zeolite-L mimic.

At the same time, a careful theoretical investigation of the structural arrangement of water in zeolite L could be relevant for improving zeolite-L-based composites and their applications. Interestingly, high-pressure overhydration experiments on zeolite L have recently evidenced a dramatic increase of the water content up to 31 H_2O molecules per unit cell (at ~ 6 GPa), against the original value of 18 [118]. Such an increase (reversible upon pressure release) is much higher compared to other aluminosilicate zeolites[49,50,119,120], and suggests a special affinity of water for zeolite L. Why is this particular zeolite so „water-friendly"? Addressing this question could impact the practical applications of zeolite-L based hybrids because water is able to displace various neutral organic dyes from zeolite L channels[101]. As a matter of fact, several dye–zeolite L materials [101,121] are destroyed by exposure to air at room temperature, which is a serious problem for hybrid composites of neutral, non carbonylic guests.

Overall, the insight gathered in this work could help both to understand the origin of the great affinity of water for zeolite L, and the role played by inclusion water on the stability of ZLMOF.

Modeling and computations

Building of the models

Zeolite L (framework type LTL, ideal unit cell stoichiometry $K_9Al_9Si_{27}O_{72}\cdot mH_2O$, s.g.*P6/mmm*). The framework is constitued by cancrinite cages stacked along the *c* axis[72,122]. This arrangement gives rise to12-membered-ring (12MR) channels with roughly circular section and 8-membered-ring (8MR) channels with smaller elliptic section, both parallel to the *c* axis. These channels are connected by a non-planar 8MR exhibiting a so-called „boat-shape". As can be seen in figure 1, the arrays of parallel 12MR channels may impart space confinement on guest species – water, in our case. Herein, we used as guess coordinates those obtained by Gigli et al. by temperature-resolved synchrot-

ron X-ray powder diffraction [116], corresponding to unit cell dimensions of *a*=18.40(4) Å and *c*=7.52(3)Å) at room temperature and pressure (figure 1).

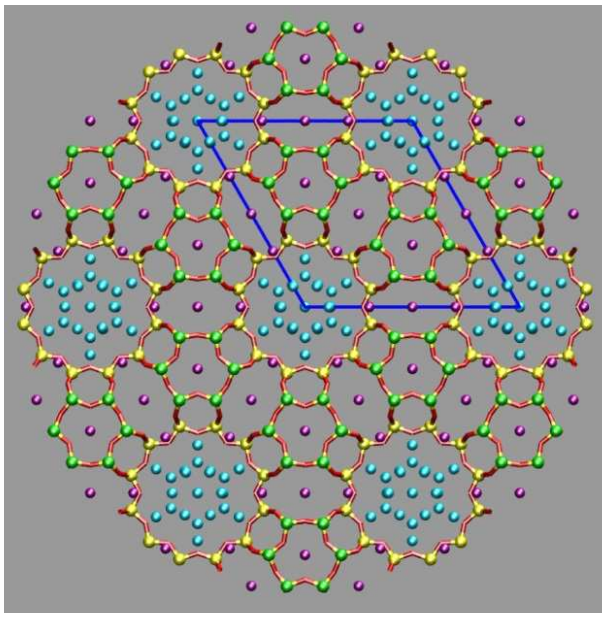

Fig. 1. Hydrated zeolite L projected in the *ab* plane from crystallographic data of ref. [116], evidencing the 6MR of the cancrinite cages, the 12MR channels and the elliptical 8MR channel (channels' axis is parallel to *c*.). The blue solid lines indicate the dimensions of the unit cell. Color codes: green, yellow = T1,T2 sites, corresponding to disordered Al, Si; red = framework oxygen sites; purple = K sites; cyan = water oxygen sites. Extraframework sites have fractional occupancy.

These authors found three types of extraframework sites for the potassium cations, located as follows: (i) at the cancrinite cage center; (ii) in the 8MR channel, between two adjacent cancrinite cages; (iii) in the 12MR channel (characterized by a maximum diameter of 10.43 Å). Only these last sites (which have fractional occupancy) can coordinate water molecules, while the remaining cationic sites are coordinated only to framework oxygens.18 water molecules per unit cell were found, distributed over five partially occupied sites [78,116]. Similar to previous observations on the natural analogue of zeolite L, perlialite [123], and on a Rb-GaSi LTL sample [124], the water molecules form clusters and cation-water layers alternating along the *c*-axis, as illustrated in figure 2. Among the 5 water sites, only two are at hydrogen-bond distance from the framework, while the other ones can only interact with H_2O's. The stoichiometry ($K_9Al_9Si_{27}O_{72}\cdot 18H_2O$) and unit cell parameters of our model were taken from Ref.[116].

In general, while diffraction analyses probe long-range order of the crystal, the presence of randomly distributed guests lowers the symmetry of the framework and results in a loss of periodicity [125]. For this reason, a fully detailed structural determination of the guests molecules is very difficult with crystallographic methods only: in most cases, the symmetry obtained by refinement should be interpreted as a configurational average over many possible disordered situation. Some consequences are the finding of guest molecules in very high-symmetry positions (which is often

an artifact) [125,126], and of multiple positions for the guests, usually in high number and with fractional occupancy, like in Ref. [116].This represents a problem for modeling, because it is necessary to single out, among the partially occupied crystallographic positions, those capable of reproducing the actual stoichiometry of the experimental system (in our case, 18 water molecules per cell), without introducing unphysical interactions (i.e. too short interatomic distances). By following these guidelines and keeping into account the (partial) occupation factors of the K sites and the water sites found by Gigli et al. [116], we set up our initial model for hydrated zeolite L.

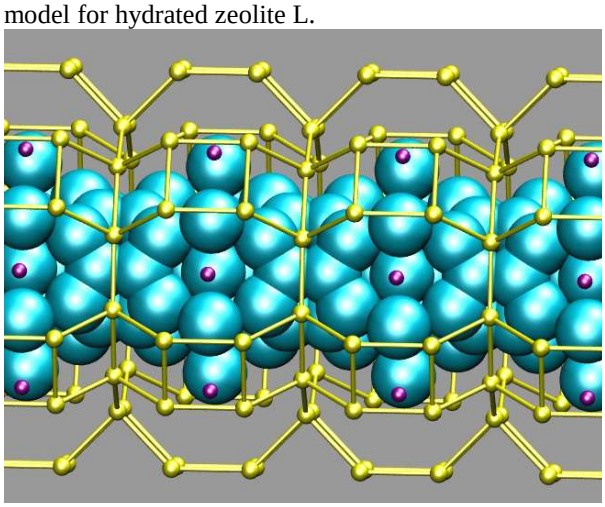

Fig. 2. Hydrated zeolite L projected in the *ac* plane (from crystallographic data of ref.[116]), representing one 12MR channel and its content (channel axis is parallel to *c*). Color codes: yellow = T1,T2 sites, corresponding to disordered Al, Si; purple spheres = K sites; cyan = water oxygen sites (in van der Waals representation). Framework oxygen sites are omitted for clarity. Extraframework sites have fractional occupancy.

ZLMOF (unit cell stoichiometry: $C_{36}H_{48}O_{31}S_{12}Ni_2Ag_8$, trigonal, space group *P*-3, *a*=15.9828(3), *c*=7.91160(10) [115]). Diffraction data collected at room pressure [115] indicate two types of silver ions (Ag1, Ag2) with the following connectivity: i) Six silver ions (Ag1) are connected to Ni *via* the ligands L (through two oxygens and two sulfur atoms); ii) Ag atoms of the second type (Ag2, occupation factor= 1/3) are bound to an oxygen and a sulfur from two L; iv) the Ni ions are surrounded by 6 ligand oxygens in a octahedral coordination, creating 3-connected nodes [115]. This connectivity generates Ni-based hexagonal channels along the *c*-axis (figure 3). The channels have maximum diameter of 11.968 Å ,which becomes narrower (7.550 Å) in correspondence of the thiomethyl groups attached to L. Each channel cavity (of 8.6 ×8.6 ×4.5 $Å^3$ size) contains a water cluster: 13 distinct crystallographic sites were found for the water oxygens. These sites have ½ occupancy, with the exception of the highly symmetric central one, for a total of 7 H_2O's per unit cell [115]. The cavities are delimited by the methyl groups of the ligands, so that the water clusters are separated from each other, as shown in figure 4.

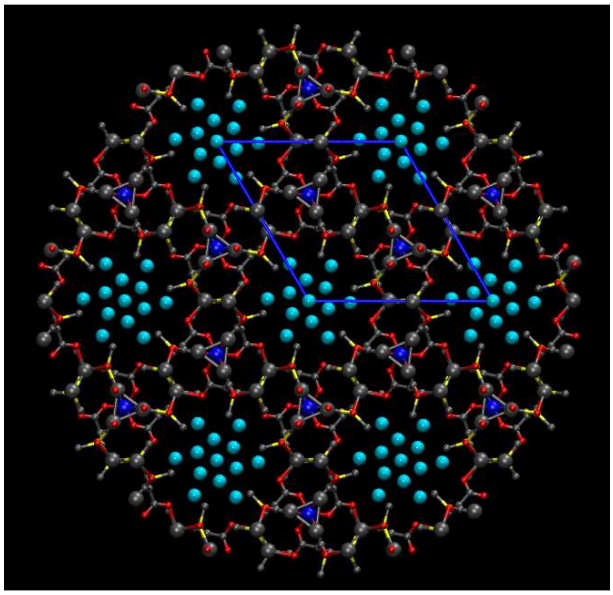

Fig. 3. ZLMOF structure projected in the *ab* plane (from crystallographic data of ref.[115]), highlighting the sections of the caterpillar-shaped nanochannels running along *c*, and the grystallographic sites of the water oxygens (cyan spheres).The blue solid lines are a guide for the eye and indicate the dimensions of the unit cell. Color codes: small gray spheres = C sites, red = framework oxygen sites; yellow= S sites; big gray spheres = Ag sites; blue = Ni sites; cyan = water oxygen sites. Ag and water sites have fractional occupancy.

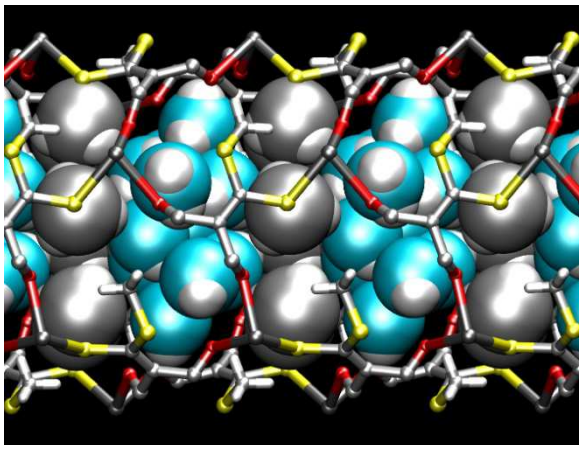

Fig. 4. ZLMOF structure projected in the *ac* plane (from crystallographic data of ref.[115]), representing one single nanochannel along *c* and its content. The 13 crystallographic sites of the water oxygens (cyan) in the channel are in the van der Waals representation. The light grey van der Waals spheres are the methyl groups of the ligands which protrude inside the channel and narrow its effective diameter. The rest of the framework is represented as sticks. Color codes: light gray = C sites, red = framework oxygen sites; yellow= S sites; dark gray spheres = Ag sites; cyan = water oxygen sites; white = H. Ni sites are not visible in this projection. Ag and water sites have fractional occupancy.

Our model has the same unit cell parameters and atomic composition as those experimentally determined, and the starting configuration was taken from the X-ray positions.The cluster $(H_2O)_7$ was built by selecting the central H_2O and, alternatively, three out of six water molecules in each of the two water rings in figure 3. Also,

as the Ag2 site occupancy is 1/3, only one of the three equivalent Ag2 positions was selected.

Computational methods

All calculations have been performed using the broadly adopted PBE approximation for DFT [127], and D2 dispersion corrections [128]. This approach (herafter indicated as "PBE-D2") is widespread in solid-state simulations of aluminosilicates because it offers a reasonable balance between computing load and accuracy level in calculating structural parameters (lattice constants, bond angles, and bond lenghts) . These features have allowed to study at atomistic level important processes in porous materials, such as pressure-driven structural changes [129], [130131], gas adsorption [132,133], catalysis [7,90,134,135] as well as interactions, properties and behavior of dye/zeolite-L composites [78,79,109 111]. The cell parameters and bond lenghts / bond angles optimized (at 0 K) with PBE-D2 reproduce satisfactorily the corresponding experimental values, as evidenced by thorough benchmarking studies of hydrated aluminosilicates [136,137] and all-silica zeotypes[138]. Tests towards higher-accuracy methods performed on silica polymorphs [139], and aluminosilicate/aluminophosphate zeotypes [130], [138,140,141] provided favorable comparison as well. Moreover, also for finite temperature conditions this approach delivers good agreement between average framework structures (from first-principles molecular dynamics) and X-ray refinement data, for different water-containing zeotypes, including zeolite L [48,131,142], [78,79,111].

The geometry optimizations were performed with the Quantum Espresso code [143]. Nonetheless, prior to optimization, several picoseconds of first principles molecular dynamics simulations were carried out at room temperature, followed by simulated annealing processes to bring slowly down the temperature of the system (i.e. the nuclear kinetic energy). Such preliminary steps were performed using the CPMD code [144].

Electronic wave functions were expanded in planewaves up to a kinetic energy cutoff of 30 Ry (240 Ry for the density). In the case of hydrated zeolite L, electron–ionic core interactions were computed with ultrasoft Vanderbilt pseudopotentials for H, C, and O and with norm conserving pseudopotentials of the Kleinman-Bylander form and nonlinear core corrections for Si, Al, and K[145–147]. This electronic structure computational scheme provided a proper description of various zeolite L hybrids [78,79,109 109–111] and other organic–inorganic materials [148–153], thus representing a well-tested strategy for the modeling of complex supramolecular systems. The PBE-D2 approach has been also widely adopted in MOFs modeling, for example to study the hydrogen and carbon dioxide adsorption sites in ZIF-8 and other isostructural systems [133], acetylene and methane adsorption in the pores of metal formates with different metal centres (Mg, Mn, Fe, Co, Zn) [154], or the gate-opening process in ZIFs of sodalite topology [155]. Also, a very recent benchmarking investigation clearly underlines that dispersion corrected PBE-based functionals provide reasonably accurate results in reproducing the structural properties of MOFs with open porosities [156].

Nonetheless, pure DFT has known limitations in treating properties such as magnetization in open-shell transition metal atoms[157,158]. A widespread and more computationally convenient way to overcome such limitations is the use of Hubbard corrections[159,160]. Hence, we enhanced the PBE-D2 approach by applying Hubbard *U* corrections to the localized d electrons of 3d transition metals. Specifically, for Ni we used a *U* value of 6.4 eV, as proposed in Ref. [161]. The electron-ionic cores interactions for all atoms in ZLMOF were treated exclusively with ultrasoft pseudopotentials [145]. Unit cell parameters were kept fixed to the experimental ones [115].

During geometry optimizations performed on both ZL and ZLMOF, all atomic coordinates were left free to move. Optimizations were considered to be converged for values of maximum force on the ions below $1.\times10^{-5}$ hartree/bohr. The Brillouin zone was sampled using a 1x1x2 mesh. In the case of ZLMOF, the open shell configuration of Ni was treated by giving independent magnetization to the two Ni atoms in the simulation cell. The two possible cases were considered: ferromagnetic arrangement (Ni1=1/2, Ni2=1/2) and antiferromagnetic arrangement (Ni1=1/2, Ni2= -1/2).

For both Zeolite L and ZLMOF, the stabilization energy of the hydrated materials with respect to the isolated components (i.e. the framework and the water molecules) was determined *via t*he following equations:

$\Delta E(ZL{\cdot}18\ H_2O)=E(ZL{\cdot}18\ H_2O) - E(\text{dry ZL}) - 18\times E(H_2O)$

$\Delta E(ZLMOF{\cdot}7\ H_2O)=E(ZLMOF{\cdot}7\ H_2O) - E(\text{dry ZLMOF}) - 7\times E(H_2O)$

Where $E(ZL{\cdot}18\ H_2O)$ / $E(ZLMOF\ 7\ H_2O)$ is the energy of the optimized hydrated ZL/hydrated ZLMOF) respectively, E(dry ZL) /E(dry ZLMOF) is the energy of the empty ZL/ZLMOF, respectively, and $E(H_2O)$ is the energy of an isolated water molecule.

In addition, to estimate the adsorption energy of a single water molecule inside the considered host materials, two further models were built and optimized, consisting of one water molecule *per* ZL and ZLMOF unit cell, respectively, using the same simulation parameters adopted for the previously described model systems. The stabilization energy of these models with respect to the isolated components was calculated as follows:

$\Delta E(ZL{\cdot}1H_2O)=E(ZL{\cdot}1H_2O) - E(\text{dry ZL}) - E(H_2O)$

$\Delta E(ZLMOF{\cdot}1H_2O)=E(ZLMOF{\cdot}1\ H_2O) - E(\text{dry ZLMOF}) - E(H_2O)$

Finally, in the data analysis performed on both systems, the following cutoff distances were assumed for evaluating hydrogen bond interactions: O-O=3.4 Å; O-H = 2.3 Å.

Results and discussion

ZLMOF

The energetics of water molecules inside ZLMOF was investigated firstly by calculating the stabilization energy of a single water molecule (per ZLMOF unit cell) with respect to the isolated constituents of the host-guest system

(namely, the water molecule and the bare ZLMOF framework). These calculations revealed that the anhydrous ZLMOF is stable, in line with the experimental observation that the ZLMOF can sustain dehydration without collapse of the framework structure [115], and that the stabilization energy of a water molecule inside ZLMOF amounts to -13.05 kcal/mol – hence, a value significantly higher than those typical of hydrogen bonds (~5 kcal/mol). Indeed, the optimized structure of ZLMOF·1H_2O evidences that the water molecule not only forms a strong hydrogen bond with a carboxylate oxygen of the ligand (1.797 Å), but it also weakly interacts with another carboxylate oxygen of the same ligand molecule (d=2.815 Å). A closer inspection of the geometry of the ligand in the dry ZLMOF and in the ZLMOF·1H_2O models reveals that the C-O distances of the oxygens involved in the interactions with water change from 1.254 Å and 1.264 Å in the dry model to 1.262 Å and 1.263 Å in the ZLMOF·1H_2O system. This result suggests that water increases the conjugation of the carboxyl groups thus imparting, besides hydrogen bonding and van der waals interactions, additional stabilization to the ZLMOFframework – in particular to the ligands.

To determine the water arrangement and the related energetics inside hydrated ZLMOF, we performed geometry optimizations of models having the same unit cell stoichiometry (namely, $C_{36}H_{48}O_{31}S_{12}Ni_2Ag_8$ 7 H_2O) but different starting distributions of the water molecules. As a general remark, the first important result of these calculations is that the structures with ferromagnetic and antiferromagnetic arrangements of the Ni ions were found to be isostructural and isoenergetic. This finding can be rationalized by noting that Ni centers are very far from each other, the closest Ni-Ni separation being 7.912 Å.

From the optimizations we obtained two configurations separated by 7.01 kcal/mol energy difference. The minimum energy structure (MIN), reported in figure 5, exhibits a ring of seven water molecules, hydrogen bonded among each other and with the framework (ligand) oxygens. The other structure (CENT, figure 6) features one molecule at the channel center, surrounded by other six H_2O‘s forming a ring; also in this case, the water molecules are hydrogen bonded both to each other and with ligand oxygens. The stabilization energies calculated for the MIN and CENT structures amount to -117.22 and to -110.21 kcal/mol, respectively.

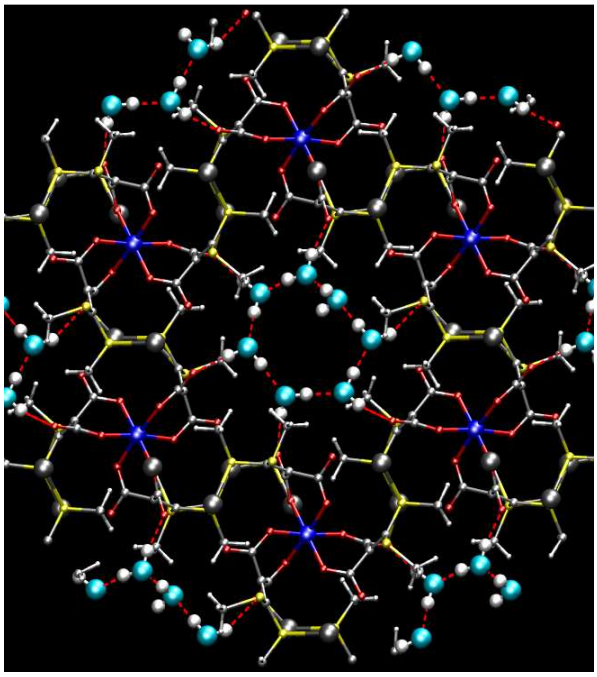

Figure 5. Minimum energy structure of hydrated ZLMOF, containing 7 water molecules per unit cell (projection in the *ab* plane). Color codes: small gray spheres = C, red = ligand oxygens; yellow= S; big gray spheres = Ag; blue = Ni; cyan = water oxygens; white=H. Hydrogen bonds are in red.

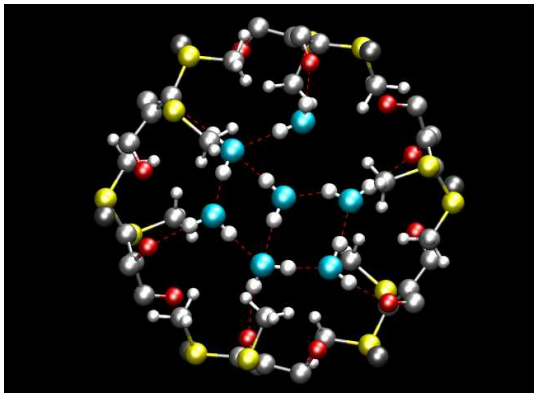

Figure 6. Hydrated ZLMOF structure (7 H_2O's per unit cell) exhibiting a water molecule at the channel center (projection in the *ab* plane). Only the H_2O's and the ligands atoms delimiting one channel are shown. Color codes: small gray spheres = C, red = ligand oxygens; yellow= S; big gray spheres = Ag; cyan = water oxygens; white=H. Hydrogen bonds are in red.

This means that the energetic stabilization of a single water molecule in the MIN and CENT structure amounts to -16.75 and -15.74 kcal/mole, respectively: hence, even greater than that found for a single water molecule hosted in ZLMOF (-13.05 kcal/mol). This result is interesting, because it indicates that the stabilization of a water molecule in ZLMOF increaseswith the water content, due to the formation of water-water hydrogen bonds, and presumably also to the strenghtening of the water-ZLMOF stabilizing interactions in the as-prepared material with respect to ZLMOF·$1H_2O$ system.
Intriguigly, in both structures the water network is formed by seven hydrogen bonds, and it is connected to the channel's ligand oxygens by six hydrogen bonds. If we take

the hydrogen bond distances as a measure of the strenght of hydrogen bonds, comparison of the values obtained for these two arrangements (Table 1), suggests that in the MIN structure the water network is stronger and interacts more favorably with the ZLMOF channel walls. In particular, the average water-water and water-ligand hydrogen bond distances in the minimum energy structure amount to 1.773 Å and 1.952 Å respectively. Such separations become both appreciably longer for the CENT structure – namely 1.887 Å and 2.016 Å, respectively. Therefore, the higher stability of the MIN structure with respect to CENT may be ascribed to the greater strenght of the hydrogen bonding network.

Table 1. Water-water and water-framework hydrogen bond distances (Å) in ZLMOF. Average values in bold.

MIN[1]			**CENT**[2]		
	Water water	Water-ligand		Water water	Water-ligand
	1.792	1.883		2.027	2.003
	1.673	2.123		1.802	1.996
	1.662	1.891		1.914	1.879
	1.778	2.093		1.680	2.226
	1.789	1.903		1.760	1.820
	1.811	1.816		1.991	2.169
	1.903			2.038	
O-H	**1.773**	**1.952**		**1.887**	**2.016**
O-O	**2.769**	**2.905**		**2.858**	**2.988**

[1]MIN= minimum energy structure (figure 5); [2]CENT=central water structure (figure 6).

Also importantly, in both structures the water-water hydrogen bonds are significantly shorter than the water-ligand oxygen ones, indicating that the water interacts more strongly with itself than with the framework. This is in line with what found for water in zeolites, mesoporous silicas, or layered materials. Indeed, the predominance of the water-water interactions is a rather general aspect of the collective properties of water when confined in nanosized cavities, irrespective from the hydrophobic or hydrophilic character of the enviroment [1].

Table 2. Metal-ligand distances (Å) in ZLMOF.

MIN[1]			**CENT**[2]		
	Ag1-O	**Ag1-S**		**Ag1-O**	**Ag1-S**
	2.344	2.443		2.334	2.443
	2.726	2.505		2.762	2.489
Av	**2.535**	**2.474**	**av**	**2.548**	**2.466**
Exp	*2.330*	*2.457*	*exp*	*2.330*	*2.457*
	2.537	*2.507*		*2.537*	*2.507*
exp av	***2.434***	***2.482***	***exp av***	***2.434***	***2.482***
	Ag2-O	**Ag2-S**		**Ag2-O**	**Ag2-S**
	2.305	2.507		2.285	2.493
	2.278	2.496		2.281	2.496
Av	**2.292**	**2.502**	**av**	**2.283**	**2.495**
	Ni-O	**Ni-Ag2**		**Ni-O**	**Ni-Ag2**
	2.103	3.856		2.111	3.872

	2.106	3.940		2.105	3.866
Av	**2.105**	**3.898**	**av**	**2.108**	**3.869**
exp av	*2.040*		*exp av*	*2.040*	

[1]MIN= minimum energy structure (Fig. 5); [2]CENT=central water structure (Fig. 6). Average values (av) in bold, experimental values [115] in italic. Comparison with experiment is reported only for sites with occupancy=1.

As above specifed, the water clusters do not join to form a continuous structure along the channel, as they are well separated from each other. This happens because the thiomethyl groups attached to L tighten the free diameter of the channel to 7.538 Å, well in line with the experimental value of 7.550 Å. This situation can be visually understood by observing figure 7: the methyl groups protruding inside the channel form a hydrophobic section, which prevents the formation of a continuous supramolecular water aggregate along the ZLMOF channel.

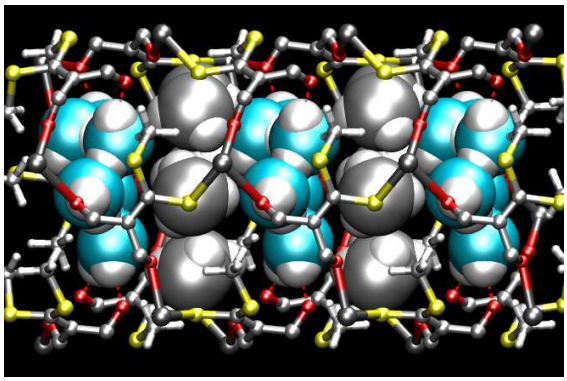

Fig. 7. Minimum energy structure of hydrated ZLMOF projected in the *ac* plane, representing one channel along *c* and its content (7 H_2O's molecules, in wan der Waals representation). The light grey van der Waals spheres are the ligands' methyl groups which protrude in the channel interior and narrow the internal diameter. The rest of the framework is shown as sticks. Color codes: light gray = C, red = framework oxygens; yellow= S; dark gray spheres = Ag; cyan = water oxygens; white = H.

Notably, the interaction of the water molecules with the ligand oxygens affects the metal-ligand coordination distances (Table 2). Indeed, each Ag1 is coordinated to two ligand oxygens, but the coordination distances are significantly different: there is a longer one, 2.726 Å, and a shorter one, 2.344 Å – in line with what found experimentally. As shown by the data in Table 2, both MIN and CENT structures share this feature. The longest Ag1-O distances always involve the ligand oxygens forming a hydrogen bond with a water proton. Hence, interaction of a ligand oxygen with water through hydrogen bonding has the effect of weakening the coordination of this oxygen to the metal center.
Although to a lesser extent, also the two Ag1-S distances differ: each Ag1 is bound to two sulphur atoms with coordination distances of 2.505 Å and 2.443 Å, respectively. Compared to the Ag1-O case, the much lower difference between the Ag1-S distances can be explained by noting that, unlike oygens, the sulfur atoms of the ligands do not directly interact with water molecules through hydrogen bonding.

Similarly, water molecules are not hydrogen bonded to the coordination environments of Ag2 and Ni, and their structural effects are therefore barely significant (see Table 2). For instance, the average Ni-O coordination distances in the MIN and CENT structure are very similar (2.105 and 2.108 Å, respectively) in spite of the different arrangement of water (cfr. figures 5 and 6).
In summary, three main points emerge from our analysis: i)the stabilization energy *per* water molecule increases with the water content – i.e. in passing from ZLMOF·1H_2O to ZLMOF·7H_2O; ii) waters in ZLMOF are strongly bound with themselves and less strongly with the ligands; iii) the presence of water essentially affects the coordination of Ag1 via hydrogen bond with one ligand oxygen, resulting into a weaker Ag1-O bond.
Taken as a whole, these results rationalize two remarkable experimental observations: i) the stability of the water aggregate (desorption occurs at ~125 °C); ii) ZLMOF resistance to water removal [115]. Indeed, besides the stabilizing hydrogen-bond interactions and water-induced conjugation enhancement of the ligand carboxyl groups, the resilience of the supramolecular water clusters towards desorption is also due to their strict confinement in individual cavities, which act as a protective environment towards external agents or high temperature conditions. Also, the weak interaction of water with the metal coordination environment ensures that water removal would not drastically affect the stability of the ZLMOF framework.

Zeolite L

Similarly to ZLMOF, in order to assess the energetics,we calculated the stabilization energy of one water molecule (per ZL unit cell) with respect to the isolated water molecule and bare ZL framework. We found that this quantity amounts to -20.42 kcal/mol – a value well in line with those reported in previous studies on water in ZL. This value is sensibly higher than the energy of a water molecule in ZLMOF because of the strong interaction of water with ZL K^+ cations. Indeed, the optimized structure of ZL·1H_2O evidences that the water molecule not only forms a strong hydrogen bond with a carboxylate oxygen of the ligand (1.866 Å), but it is also strongly bound to an extraframework potassium cation (d=2.716 Å).
The minimum energy structure calculated for hydrated zeolite L(figure 8) is stabilized by-326.74 kcal/mole with respect to the isolated components: this indicates that the stabilization energy of a single water molecule in ZL amounts to-18.15 kcal/mol. This value is only slightly higher than the corresponding value (-16.75 kcal/mol) found for ZLMOF at the same conditions, and, remarkably, is lower than the stabilization of a single water molecule in the LTL framework. Hence, the present energetic analysis highlights that the energy stabilization of a water molecule decreases with the water content in zeolite L, following thus an opposite trend respect to that found for ZLMOF. As deduced from the minimum energy geometry, the reason for this behaviour lies mainly in the increased competition of water molecules to bind with the potassium cations in the

ZL·18 H_2O hydrated material. This system has a network of hydrogen bonds more extended and complex with respect to ZLMOF, due to the greater number of water molecules per unit cell. In addition to water and framework oxygens, the network involves K^+ cations as well: the extraframework cations play a mayor role in governing the organization of water in zeolites [1,162,163], and zeolite L is no exception[102,105]. In this view, we thorougly analyze the connectivity of the water aggregates starting from the environment of potassium cations.

In our model, 4 of the 6 available K sites close to the main 12MR channel (KD sites according to Gigli et al, with 3.8 occupancy[116]) are occupied by potassium cations. These K^+ are the only ones that can interact with water. Each K^+ is coordinated to at least two water molecules and five framework oxygens, with an average coordination number of 7.75 (assuming a cutoff distance of 3.2 Å) . Specifically, two K^+ are coordinated to 2 water molecules (average K-O distance: 2.734 Å) and the other two to three H_2O's, with average distance of 2.758 Å (Table 3).

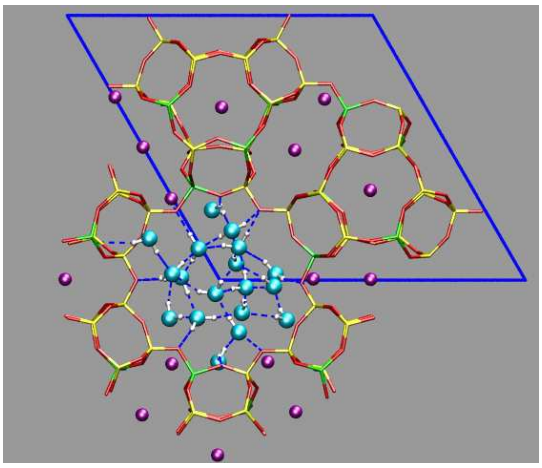

Fig. 8. Minimum energy structure of hydrated zeolite L (ZL·18 H_2O)projected in the *ab* plane. The blue solid lines indicate the unit cell. Color codes: yellow = Si, green = Al, red = framework oxygens; purple = K; cyan = water oxygens, white=H. Blue dashed lines indicate the hydrogen bonds.

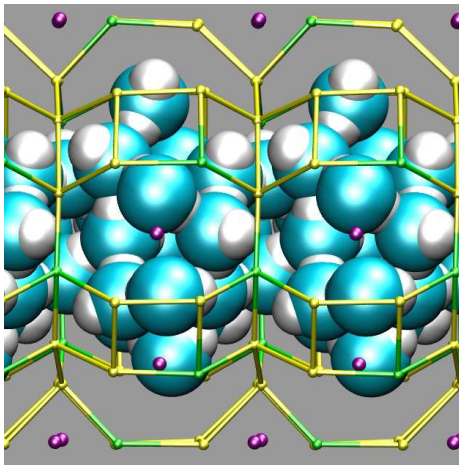

Fig. 9. Minimum energy structure of hydrated zeolite L (ZL·18 H_2O) projected in the *ac* plane, representing one single channel along *c* and its content (18 H_2O's per unit cell). Colors: yellow = Si, green = Al, purple = K, cyan = water O, white=H. Framework O omitted for clarity.

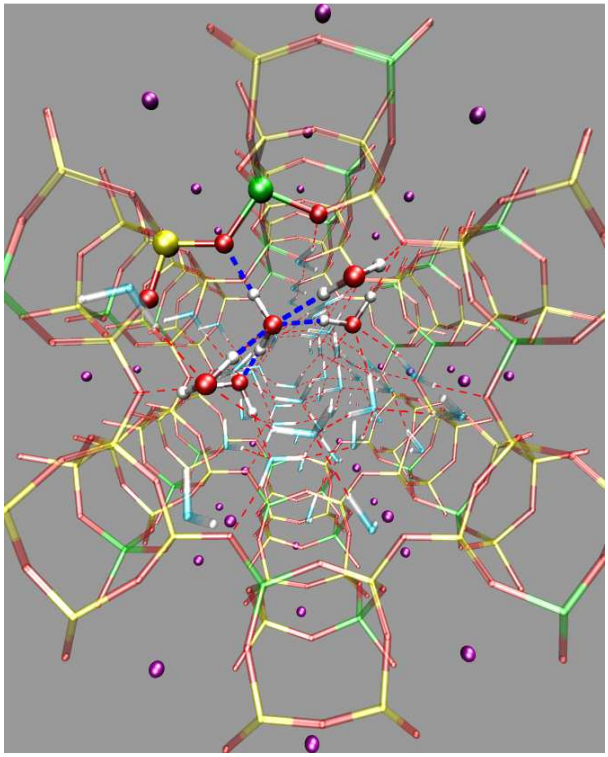

Fig. 10. Perspective view of zeolite L minimum energy structure showing the peculiar 5-hydrogen-bond (5-HB) arrangement (in ball-and-stick and dashed blue lines). 3 out of 18 H_2O's per unit cell have 5-HB. Color codes: yellow = Si, green = Al, red sticks = framework O; purple = K; cyan sticks = water O, white=H, red spheres = oxygens involved in the 5-HB structure. Blue dashed lines=5-HB, red dashed lines=the full hydrogen bonding network.

Table 3. Water-water and water-framework hydrogen bond distances (Å) in Zeolite L. Average values in bold.

Interaction	distance
K-O(2w)	**2.734**
K-O(3w)	**2.758**
O-H H-bond (K,1W))	1.754
O-H H-bond(1W)	1.556
O-H H-bond(2W)	1.804
O-H H-bond (3W)	1.920
All O(water)-H	**1.833**
All O(frame)-H	**1.953**

In total, there are 8 water molecules coordinated to the 4 K^+. Two H_2O's are bound each to two K^+ concomitantly, and therefore cannot act as acceptors of hydrogen bonds. Among the other 6 molecules, each bound to a single K^+, only two accept an hydrogen bond from a water proton, with rather short hydrogen-bond separation (average value =1.754 Å), indicating a strong interaction (Table 3). The remaining 10 water molecules per unit cell are not directly coordinated to K. Six of them accept two hydrogen bonds (average hydrogen bond distance = 1.804 Å),while one H_2O interacts with only one proton, forming a very strong hydrogen bond (O···H distance =1.555 Å). Quite surprisingly, the other three water molecules accept three hydrogen bonds each (average O···H distance = 1.920 Å).

On the whole, the network consists of 24 water-water hydrogen bonds, and only 11 water-framework hydrogen bonds. Also, as found for ZLMOF, the interactions among water molecules are stronger than the water-framework ones, being the average hydrogen bond distances equal to 1.833 Å and 1.953 Å, respectively (Table 3). On average the H-bond interactions are slightly weaker than in the ZMLOF minimum energy structure because of the strong coordination of several water oxygens (eight out of 18) to potassium cations. Sigificantly, the coordination of some of the water molecules to K also explains from a molecular viewpoint the observation of Gigli et al that water molecules were released in different steps in the 101 °C to 244 °C interval [116]. Indeed, the water molecules bonded to K are the last ones to be lost [116].
Differently from ZLMOF, the 12MR channels of zeolite L do not have hydrophobic „sections“, and so water molecules can form a continuous structure. However, the space available to water is not constant along the channel, as evidenced in figure 9: the calculated maximum and minimum diameters (without oxygen van der Waals radii) amount to 13.677 Å and 9.804 Å respectively. Therefore, the aggregate of water molecules is shaped by the internal geometry of the channel. Such a behaviour is common to confined water, especially when the confining environment is either hydrophobic, or large enough [1]. In such cases, water forms hydrogen-bonded clusters: the greater is the cluster's size, the closer the behaviour is to bulk water [164]. Here, the water molecules not bonded to K^+ mainly accept two hydrogen bonds and donate two hydrogen bonds, in a tetrahedral coordination environment similar to bulk water. Nonetheless, by observing figure 9, it appears that the channel's space is not completely filled by the 18 water molecules. Likely, additional molecules might be accomodated inside the channel via forced intrusion, thus providing a rational for the impressive increase of water content (from 18 to 31 H_2O per unit cell) recently found in pressure-induced over-hydration of zeolite L [118]. Upon confinement, the water molecules tend to aggregate in clusters, which become more stable and larger as the loading increases due to the collective properties of the water-water hydrogen bond network. Apparently, zeolite L channels provide enough room not only for the formation of the 18 H_2O aggregate at room conditions, but also for its enlargement via pressure-induced water intrusion.

Table 4. Hydrogen bond distances (Å) for the 3 water molecules in Zeolite L channels with pentacoordinated hydrogen bonding environment. Average values in bold.

Interaction	water1	water2	water3
HB donor to O framework	1.646	1.842	2.031
HB donor to O water	1.555	1.771	1.811
HB acceptor	1.811	1.882	2.223
HB acceptor	1.884	2.002	1.960
HB acceptor	1.771	1.900	1.811
Average HB distance	**1.733**	**1.867**	**1.986**

The water supramolecular organization in zeolite L also features significant deviations from the tetrahedral bulk-

water coordination. As reported in Table 4, three water molecules (water1, water2, water3) have an unusual 5-hydrogen bond arrangement, resulting into a square pyramidal coordination geometry, as shown in figure 10 for water1. Specifically, the two hydrogen bonds where water1 acts as donor have lenghts of 1.646 and 1.555 Å, while the remaining three ones (where water1 acts as acceptor) are 1.811, 1.884 and 1.771 Å, respectively. These five hydrogen bonds average to 1.733 Å, indicating that the interactions experienced by this 5-hydrogen bonded water are particularly strong. Interestingly, a similar square-pyramidal „hypercoordinated" geometry is found in the anionic hydrogen bonded complex ($H_9O_5^-$) [165,166], which is one of the dominant solvation structures for the OH^- ion in aqueous hydroxyde solutions [167].
Although to lesser extent, also water2 and water3 present a similarly strong hydrogen bonding environment, with average over the 5 hydrogen bond distances equal to 1.867 Å and 1.986 Å, respectively. Note that all of three water molecules donate a hydrogen bond to a framework oxygen, located in a Si-O-Al bridge for water1, and in a Si-O-Si bridge for water2/water3. The greater strenght of water1 hydrogen bonding environment may thus be ascribed to its direct interaction with an Al-bonded bridging oxygen – which is well known to have Brønsted base character [168]. Hence, all the hydrogen bond interactions are emphasised, causing an appreciable weakening of the O-H covalent bonds of water1. Specifically the bond distances of water1 are 1.006 Å and 1.032 Å: while the first proton is hydrogen bonded to the Si-O-Al bridge, the second one is at very close distance (1.556 Å) with a water accepting one single, very strong hydrogen bond (Table 3). The combination of these two „solvated" water molecules – i.e. the 5-hydrogen-bonded water1 and the close acceptor molecule, along with their surrounding hydrogen bond network –might thus be considered similar to a „pre-dissociated" state in bulk water. Notably, the above results are extracted from a 0 K minimum energy structure. Presumably, both temperature and quantum effects (e.g.proton tunneling and/or zero point energy) may lead to actual water dissociation. This event is most likely facilitated by a favorable pre-alignment of water molecules. Water alignment has been often detected in confined spaces[169], from the one-dimensional channels of bikitaite and Li-ABW zeolites [25–27,29,34–37,170], to carbon nanotubes [171], whereas in bulk liquid water a reshuffling of the hydrogen bonding network is needed before proton transfer could take place. The peculiar local conformation of hydrogen bonds within the channels of zeolite L, involving a hypercoordinated water molecule, appears therefore to be functional to the experimentally detected water ionization under confinement. Indeed, Calzaferri et al. reported the ionic strength inside of the channels to be very high and acidic in hydrated zeolite L, and ascribed this phenomenon to a water self-ionization mechanism [172]. Our simulations, which have highlighted a possible precursor structure for a fully-ionized pair of water molecules, support such an interpretation and might provide further insight on the microscopic details of this process.

Conclusion

We have analyzed the hydrogen bonding pattern of water molecules included in zeolite L and in its ZLMOF mimic. Whereas water molecules in zeolite L form a continuous structure inside the channel, the arrangement of water in ZLMOF is more similar to a row of isolated water clusters. This depends on the different composition of the two materials, as well as on the different internal geometry of the channels. We showed that water molecules impart a significant energetic stabilization to the ZLMOF framework, which increases with the water content. Moreover, water clusters in ZLMOF are formed by strongly hydrogen bonded molecules, which also interact – but more weakly – with the channels‘ walls. This microscopic picture of the host-guest interactions explains why ZLMOF can withstand water removal, and might support the template-role of the water clusters during the synthesis. The narrowing of the internal diameter of the ZLMOF channels due to ligands‘ thiomethyl groups should likely disfavour the incorporation of long photoactive molecules such as perylene-dimmide dyes. On the other hand, the well-defined ZLMOF cavities may provide a kind of „isolated supramolecule“ environment with regular size for the protection of e.g. small metal clusters with interesting electro-optical, catalytic or magnetic properties. Also, ZLMOF itself shows interesting intrachannel photochemistry: it catalyzes the reduction of paranitrofenol and its activity greatly increases when coated with silver nanoparticles[115]. With these premises, the inclusion of very small metal clusters within individual ZLMOF cages might be an intriguing development.

The one dimensional confining environment of zeolite L nanochannels, at difference from ZLMOF, is not interrupted by idrophobic sections. Hence, water molecules in zeolite L can form a continuous supramolecular structure, shaped by the internal geometry of the channel and kept together by a complex network of intermolecular interactions. The energy stabilization of water in zeolite L is slightly higher than in ZLMOF, but decreases by increasing the water content. Although coordination to potassium cations is energetically predominant, key roles are also played by the Brønsted basicity of Al-O-Si framework oxygens, and by the water-water interactions, which also exhibit both low-coordinated and hyper-coordinated conformations. The peculiar local arrangement with a 5-hydrogen bonded zeolitic water, showed herein for the first time, may facilitate proton transfer and can thus be regarded as a water pre-dissociation complex. Hence, con-finement-driven hypercoordination of zeolitic water appears to be the molecular level origin of the experimentally detec-ted high proton activity in zeolite L nanochannels.

Acknowledgements. This work was supported by the Italian MIUR, within the frame of the following projects: PRIN2015 “ZAPPING” (2015HK93L7), ImPACT (FIRB RBFR12CLQD), and University of Insubria Far 2016-2017.

References

(1) Tabacchi, G. Supramolecular Organization in Confined Nanospaces. *ChemPhysChem* **2018**, *19* (11), 1249–1297.

(2) Corma, A.; Garcia, H. Supramolecular Host-Guest Systems in Zeolites Prepared by Ship-in-a-Bottle Synthesis. *Eur. J. Inorg. Chem.* **2004**, *2004* (6), 1143–1164.

(3) Alarcos, N.; Cohen, B.; Ziółek, M.; Douhal, A. Photochemistry and Photophysics in Silica-Based Materials: Ultrafast and Single Molecule Spectroscopy Observation. *Chem. Rev.* **2017**, *117* (22), 13639–13720.

(4) Xing, P.; Yang, C.; Wang, Y.; Phua, S. Z. F.; Zhao, Y. Solvent-Controlled Assembly of Aromatic Glutamic Dendrimers for Efficient Luminescent Color Conversion. *Adv. Funct. Mater.* **2018**, *28* (34), 1802859.

(5) Calzaferri, G.; Huber, S.; Maas, H.; Minkowski, C. Host-Guest Antenna Materials. *Angew. Chemie - Int. Ed.* **2003**, *42* (32), 3732–3758.

(6) Hashimoto, S.; Samata, K.; Shoji, T.; Taira, N.; Tomita, T.; Matsuo, S. Preparation of Large-Scale 2D Zeolite Crystal Array Structures to Achieve Optical Functionality. *Microporous Mesoporous Mater.* **2009**, *117* (1–2), 220–227.

(7) Garcia, H.; Parvulescu, V. I. Heterogeneous Catalysis Based on the Supramolecular Association. *Catal. Sci. Technol.* **2018**, *8* (19), 4834–4857.

(8) Zendehdel, M.; Bodaghifard, M. A.; Behyar, H.; Mortezaei, Z. Alkylaminopyridine-Grafted on HY Zeolite: Preparation, Characterization and Application in Synthesis of 4 H -Chromenes. *Microporous Mesoporous Mater.* **2018**, *266*, 83–89.

(9) Calzaferri, G. Nanochannels: Hosts for the Supramolecular Organization of Molecules and Complexes. *Langmuir* **2012**, *28* (15), 6216–6231.

(10) Kim, H. S.; Yoon, K. B. Preparation and Characterization of CdS and PbS Quantum Dots in Zeolite Y and Their Applications for Nonlinear Optical Materials and Solar Cell. *Coord. Chem. Rev.* **2014**, *263–264* (1), 239–256.

(11) Ozin, G. A.; Kuperman, A.; Stein, A. [Review]Advanced Zeolite, Materials Science. *Angew. Chemie Int. Ed. English* **1989**, *28* (3), 359–376.

(12) Seifert, R.; Kunzmann, A.; Calzaferri, G. The Yellow Color of Silver-Containing Zeolite A. *Angew. Chemie Int. Ed.* **1998**, *37* (11), 1521–1524.

(13) Baldansuren, A.; Roduner, E. EPR Experiments of Ag Species Supported on NaA. *Chem. Phys. Lett.* **2009**, *473* (1–3), 135–137.

(14) Heo, N. H.; Kim, Y.; Kim, J. J.; Seff, K. Surprising Intrazeolitic Chemistry of Silver. *J. Phys. Chem. C* **2016**, *120* (10), 5277–5287.

(15) Ramachandra, S.; Popovicâ, Z. D.; Schuermann, K. C.; Cucinotta, F.; Calzaferri, G.; De Cola, L. Förster Resonance Energy Transfer in Quantum Dot-Dye-Loaded Zeolite L Nanoassemblies. *Small* **2011**, *7* (10), 1488–1494.

(16) Moon, D. J.; Lim, W. T.; Seff, K. Structures of the Subnanometer Clusters of Cadmium Sulfide Encapsulated in Zeolite Y: Cd4S6+and Cd(SHCd)46+. *J. Phys. Chem. C* **2016**, *120* (30), 16722–16731.

(17) Li, H.; Li, P. Luminescent Materials of Lanthanoid Complexes Hosted in Zeolites. *Chem. Commun.* **2018**.

(18) Woodtli, P.; Giger, S.; Müller, P.; Sägesser, L.; Zucchetto, N.; Reber, M. J.; Ecker, A.; Brühwiler, D. Indigo in the Nanochannels of Zeolite L: Towards a New Type of Colorant. *Dye. Pigment.* **2018**, *149*, 456–461.

(19) Devaux, A.; Cucinotta, F.; Kehr, S.; Cola, L. De.

Functionalization and Assembling of Inorganic Nanocontainers for Optical and Biomedical Applications. In *Functional Supramolecular Architectures*; WILEY-VCH Verlag & Co. KGaA: Weinheim, Germany, 2014; pp 281–342.

(20) Zaarour, M.; Dong, B.; Naydenova, I.; Retoux, R.; Mintova, S. Progress in Zeolite Synthesis Promotes Advanced Applications. *Microporous Mesoporous Mater.* **2014**, *189*, 11–21.

(21) Demontis, P.; Stara, G.; Suffritti, G. B. Behavior of Water in the Hydrophobic Zeolite Silicalite at Different Temperatures. A Molecular Dynamics Study. *J. Phys. Chem. B* **2003**, *107* (18), 4426–4436.

(22) Torres, C.; Gulín-González, J.; Navas-Conyedo, E.; Demontis, P.; Suffritti, G. B. The Behavior of Silicalite-1 under High Pressure Conditions Studied by Computational Simulation. *Struct. Chem.* **2013**, *24* (3), 909–915.

(23) Zhou, T.; Bai, P.; Siepmann, J. I.; Clark, A. E. Deconstructing the Confinement Effect upon the Organization and Dynamics of Water in Hydrophobic Nanoporous Materials: Lessons Learned from Zeolites. *J. Phys. Chem. C* **2017**, *121* (40), 22015–22024.

(24) Ståhl, K.; Kvick, Å.; Ghose, S. One-Dimensional Water Chain in the Zeolite Bikitaite: Neutron Diffraction Study at 13 and 295 K. *Zeolites* **1989**, *9* (4), 303–311.

(25) Quartieri, S.; Sani, A.; Vezzalini, G.; Galli, E.; Fois, E.; Gamba, A.; Tabacchi, G. One-Dimensional Ice in Bikitaite: Single-Crystal X-Ray Diffraction, Infra-Red Spectroscopy and Ab-Initio Molecular Dynamics Studies. *Microporous Mesoporous Mater.* **1999**, *30* (1), 77–87.

(26) Fois, E.; Tabacchi, G.; Quartieri, S.; Vezzalini, G. Dipolar Host/Guest Interactions and Geometrical Confinement at the Basis of the Stability of One-Dimensional Ice in Zeolite Bikitaite. *J. Chem. Phys.* **1999**, *111* (1), 355–359.

(27) Demontis, P.; Stara, G.; Suffritti, G. B. Dynamical Behavior of One-Dimensional Water Molecule Chains in Zeolites: Nanosecond Time-Scale Molecular Dynamics Simulations of Bikitaite. *J. Chem. Phys.* **2004**, *120* (19), 9233–9244.

(28) Ceriani, C.; Fois, E.; Gamba, A.; Tabacchi, G.; Ferro, O.; Quartieri, S.; Vezzalini, G. Dehydration Dynamics of Bikitaite: Part II. Ab Initio Molecular Dynamics Study. *Am. Mineral.* **2004**, *89* (1), 102–109.

(29) Ferro, O.; Quartieri, S.; Vezzalini, G.; Fois, E.; Gamba, A.; Tabacchi, G. High-Pressure Behavior of Bikitaite: An Integrated Theoretical and Experimental Approach. *Am. Mineral.* **2002**, *87* (10), 1415–1425.

(30) Comodi, P.; Gatta, G. D.; Zanazzi, P. F. Effects of Pressure on the Structure of Bikitaite. *Eur. J. Mineral.* **2003**, *15* (2), 247–255.

(31) Fois, E.; Gamba, A.; Tabacchi, G.; Ferro, O.; Quartieri, S.; Vezzalini, G. A Theoretical Investigation on Pressure-Induced Changes in the Vibrational Spectrum of Zeolite Bikitaite. *Stud. Surf. Sci. Catal.* **2002**, *142 B*, 1877–1884.

(32) Kolesov, B. A.; Geiger, C. A. Raman Spectroscopic Study of H 2 O in Bikitaite : " One-Dimensional Ice ." *Am. Mineral.* **2002**, *87* (10), 1426–1431.

(33) Seryotkin, Y. V. Evolution of the Bikitaite Structure at High Pressure: A Single-Crystal X-Ray Diffraction Study. *Microporous Mesoporous Mater.* **2016**, *226*, 415–423.

(34) Fois, E.; Gamba, A.; Tabacchi, G.; Quartieri, S.; Vezzalini, G. Water Molecules in Single File: First-Principles Studies of One-Dimensional Water Chains in Zeolites. *J. Phys. Chem. B* **2001**, *105* (15), 3012–3016.

(35) Fois, E.; Gamba, A.; Tabacchi, G.; Quartieri, S.; Vezzalini, G. On the Collective Properties of Water Molecules in One-Dimensional Zeolitic Channels. *Phys. Chem. Chem. Phys.* **2001**, *3* (18), 4158–4163.
(36) Fois, E.; Gamba, A.; Medici, C.; Tabacchi, G.; Quartieri, S.; Mazzucato, E.; Arletti, R.; Vezzalini, G.; Dmitriev, V. High Pressure Deformation Mechanism of Li-ABW: Synchrotron XRPD Study and Ab Initio Molecular Dynamics Simulations. *Microporous Mesoporous Mater.* **2008**, *115* (3), 267–280.
(37) Demontis, P.; Stara, G.; Suffritti, G. B. Molecular Dynamics Simulation of Anomalous Diffusion of One-Dimensional Water Molecule Chains in Li-ABW Zeolite. *Microporous Mesoporous Mater.* **2005**, *86* (1–3), 166–175.
(38) Norby, P.; Christensen, A. N.; Andersen, I. G. K.; Hjuler, H. A.; von Barner, J. H.; Bjerrum, N. J.; Tokii, T.; Zingaro, R. A. Hydrothermal Preparation of Zeolite Li--A(BW), LiAlSiO4.H2O, and Structure Determination from Powder Diffraction Data by Direct Methods. *Acta Chem. Scand.* **1986**, *40a*, 500–506.
(39) Coudert, F.-X.; Vuilleumier, R.; Boutin, A. Dipole Moment, Hydrogen Bonding and IR Spectrum of Confined Water. *ChemPhysChem* **2006**, *7* (12), 2464–2467.
(40) Gómez-Álvarez, P.; Calero, S. Insights into the Microscopic Behaviour of Nanoconfined Water: Host Structure and Thermal Effects. *CrystEngComm* **2015**, *17* (2), 412–421.
(41) Demontis, P.; Gulín-González, J.; Jobic, H.; Suffritti, G. B. Diffusion of Water in Zeolites Na A and NaCa A: A Molecular Dynamics Simulation Study. *J. Phys. Chem. C* **2010**, *114* (43), 18612–18621.
(42) McCusker, L. B.; Baerlocher, C.; Jahn, E.; Bülow, M. The Triple Helix inside the Large-Pore Aluminophosphate Molecular Sieve VPI-5. *Zeolites* **1991**, *11* (4), 308–313.
(43) Fois, E.; Gamba, A.; Tilocca, A. Structure and Dynamics of the Flexible Triple Helix of Water inside VPI-5 Molecular Sieves. *J. Phys. Chem. B* **2002**, *106* (18), 4806–4812.
(44) Alabarse, F. G.; Haines, J.; Cambon, O.; Levelut, C.; Bourgogne, D.; Haidoux, A.; Granier, D.; Coasne, B. Freezing of Water Confined at the Nanoscale. *Phys. Rev. Lett.* **2012**, *109* (3), 035701.
(45) Fois, E.; Gamba, A.; Tabacchi, G.; Quartieri, S.; Arletti, R.; Vezzalini, G. High-Pressure Behaviour of Yugawaralite at Different Water Content: An Ab Initio Study. *Stud. Surf. Sci. Catal.* **2005**, *155*, 271–280.
(46) Betti, C.; Fois, E.; Mazzucato, E.; Medici, C.; Quartieri, S.; Tabacchi, G.; Vezzalini, G.; Dmitriev, V. Gismondine under HP: Deformation Mechanism and Re-Organization of the Extra-Framework Species. *Microporous Mesoporous Mater.* **2007**, *103* (1–3), 190–209.
(47) Gatta, G. D.; Lee, Y. Zeolites at High Pressure: A Review. *Mineral. Mag.* **2014**, *78* (2), 267–291.
(48) Arletti, R.; Fois, E.; Gigli, L.; Vezzalini, G.; Quartieri, S.; Tabacchi, G. Irreversible Conversion of a Water–Ethanol Solution into an Organized Two-Dimensional Network of Alternating Supramolecular Units in a Hydrophobic Zeolite under Pressure. *Angew. Chemie - Int. Ed.* **2017**, *56* (8), 2105–2109.
(49) Gatta, G. D.; Lotti, P.; Tabacchi, G. The Effect of Pressure on Open-Framework Silicates: Elastic Behaviour and Crystal–fluid Interaction. *Phys. Chem. Miner.* **2018**, *45* (2), 115–138.
(50) Kim, Y.; Choi, J.; Vogt, T.; Lee, Y. Structuration under

Pressure: Spatial Separation of Inserted Water during Pressure-Induced Hydration in Mesolite. *Am. Mineral.* **2018**, *103* (1), 175–178.
(51) Fois, E.; Gamba, A.; Tabacchi, G.; Arletti, R.; Quartieri, S.; Vezzalini, G. The “Template” Effect of the Extra-Framework Content on Zeolite Compression: The Case of Yugawaralite. *Am. Mineral.* **2005**, *90* (1), 28–35.
(52) Gatta, G. D. Does Porous Mean Soft? On the Elastic Behaviour and Structural Evolution of Zeolites under Pressure. *Zeitschrift fur Krist.* **2008**, *223* (1–2), 160–170.
(53) Marqueño, T.; Santamaria-Perez, D.; Ruiz-Fuertes, J.; Chuliá-Jordán, R.; Jordá, J. L.; Rey, F.; McGuire, C.; Kavner, A.; MacLeod, S.; Daisenberger, D.; et al. An Ultrahigh CO_2 -Loaded Silicalite-1 Zeolite: Structural Stability and Physical Properties at High Pressures and Temperatures. *Inorg. Chem.* **2018**, *57* (11), 6447–6455.
(54) Lee, Y.; Kao, C. C.; Kim, S. J.; Lee, H. H.; Lee, D. R.; Shin, T. J.; Choi, J. Y. Water Nanostructures Confined inside the Quasi-One-Dimensional Channels of LTL Zeolite. *Chem. Mater.* **2007**, *19* (25), 6252–6257.
(55) Smirnov, K. S.; Bougeard, D. Water Behaviour in Nanoporous Aluminosilicates. *J. Phys. Condens. Matter* **2010**, *22* (28), 284115.
(56) Fois, E.; Tabacchi, G.; Devaux, A.; Belser, P.; Brühwiler, D.; Calzaferri, G. Host-Guest Interactions and Orientation of Dyes in the One-Dimensional Channels of Zeolite L. *Langmuir* **2013**, *29* (29), 9188–9198.
(57) Brühwiler, D.; Calzaferri, G.; Torres, T.; Ramm, J. H.; Gartmann, N.; Dieu, L.-Q.; López-Duarte, I.; Martínez-Díaz, M. V. Nanochannels for Supramolecular Organization of Luminescent Guests. *J. Mater. Chem.* **2009**, *19* (43), 8040–8067.
(58) Zucchetto, N.; Brühwiler, D. Strategies for Localizing Multiple Functional Groups in Mesoporous Silica Particles through a One-Pot Synthesis. *Chem. Mater.* **2018**, *30* (20), 7280–7286.
(59) Onida, B.; Bonelli, B.; Flora, L.; Geobaldo, F.; Arean, C. O.; Garrone, E. Permeability of Micelles in Surfactant-Containing MCM-41 Silica as Monitored by Embedded Dye Molecules. *Chem. Commun. (Camb).* **2001**, *0* (21), 2216–2217.
(60) Cucinotta, F.; Carniato, F.; Devaux, A.; De Cola, L.; Marchese, L. Efficient Photoinduced Energy Transfer in a Newly Developed Hybrid SBA-15 Photonic Antenna. *Chem. - A Eur. J.* **2012**, *18* (48), 15310–15315.
(61) Bagnall, A. J.; Santana Vega, M.; Martinelli, J.; Djanashvili, K.; Cucinotta, F. Mesoscopic FRET Antenna Materials by Self-Assembling Iridium(III) Complexes and BODIPY Dyes. *Chem. - A Eur. J.* **2018**, *24* (46), 11992–11999.
(62) Cucinotta, F.; Jarman, B. P.; Caplan, C.; Cooper, S. J.; Riggs, H. J.; Martinelli, J.; Djanashvili, K.; La Mazza, E.; Puntoriero, F. Light-Harvesting Antennae Using the Host-Guest Chemistry of Mesoporous Organosilica. *ChemPhotoChem* **2017**.
(63) Giustetto, R.; Seenivasan, K.; Bonino, F.; Ricchiardi, G.; Bordiga, S.; Chierotti, M. R.; Gobetto, R. Host/Guest Interactions in a Sepiolite-Based Maya Blue Pigment: A Spectroscopic Study. *J. Phys. Chem. C* **2011**, *115* (34), 16764–16776.
(64) Fois, E.; Gamba, A.; Tilocca, A. On the Unusual Stability of Maya Blue Paint: Molecular Dynamics Simulations. *Microporous Mesoporous Mater.* **2003**, *57* (3), 263–272.
(65) Costa, A. L.; Gomes, A. C.; Pereira, R. C.; Pillinger, M.; Gonçalves, I. S.; Pineiro, M.; Seixas de Melo, J. S. Interactions and Supramolecular Organization of Sulfonated Indigo and Thioindigo Dyes in Layered

Hydroxide Hosts. *Langmuir* **2018**, *34* (1), 453–464.
(66) Epelde-Elezcano, N.; Martínez-Martínez, V.; Duque-Redondo, E.; Temiño, I.; Manzano, H.; López-Arbeloa, I. Strategies for Modulating the Luminescence Properties of Pyronin Y Dye–clay Films: An Experimental and Theoretical Study. *Phys. Chem. Chem. Phys.* **2016**, *18* (12), 8730–8738.
(67) Medishetty, R.; Zaręba, J. K.; Mayer, D.; Samoć, M.; Fischer, R. A. Nonlinear Optical Properties, Upconversion and Lasing in Metal Organic Frameworks. *Chem. Soc. Rev.* **2017**, *46*, 4976–5004.
(68) Kittikhunnatham, P.; Som, B.; Rassolov, V.; Stolte, M.; Würthner, F.; Shimizu, L. S.; Greytak, A. B. Fluorescence Polarization Measurements to Probe Alignment of a Bithiophene Dye in One-Dimensional Channels of Self-Assembled Phenylethynylene Bis-Urea Macrocycle Crystals. *J. Phys. Chem. C* **2017**, *121* (33), 18102–18109.
(69) Sun, L.; Xing, H.; Liang, Z.; Yu, J.; Xu, R. A 4 + 4 Strategy for Synthesis of Zeolitic Metal–organic Frameworks: An Indium-MOF with SOD Topology as a Light-Harvesting Antenna. *Chem. Commun.* **2013**, *49* (95), 11155–11157.
(70) Noh, T. H.; Lee, H.; Jang, J.; Jung, O. S. Organization and Energy Transfer of Fused Aromatic Hydrocarbon Guests within Anion-Confining Nanochannel MOFs. *Angew. Chemie - Int. Ed.* **2015**, *54* (32), 9284–9288.
(71) Noh, T. H.; Jung, O. S. Recent Advances in Various Metal-Organic Channels for Photochemistry beyond Confined Spaces. *Acc. Chem. Res.* **2016**, *49* (9), 1835–1843.
(72) Baerlocher, C.; McCusker, L. B.; Olson, D. H. *Atlas of Zeolite Framework Types*; Published on behalf of the Structure Commission of the International Zeolite Association by Elsevier, 2007.
(73) Maas, H.; Calzaferri, G. Trapping Energy from and Injecting Energy into Dye-Zeolite Nanoantennae. *Angew. Chemie - Int. Ed.* **2002**, *41* (13), 2284–2288.
(74) Calzaferri, G. Artificial Photosynthesis. *Top. Catal.* **2010**, *53* (3–4), 130–140.
(75) Manzano, H.; Gartzia-Rivero, L.; Bañuelos, J.; López-Arbeloa, I. Ultraviolet-Visible Dual Absorption by Single BODIPY Dye Confined in LTL Zeolite Nanochannels. *J. Phys. Chem. C* **2013**, *117* (25), 13331–13336.
(76) Li, H.; Wang, Y.; Zhang, W.; Liu, B.; Calzaferri, G. Fabrication of Oriented Zeolite L Monolayers Employing Luminescent Perylenediimide-Bridged Silsesquioxane Precursor as the Covalent Linker. *Chem. Commun. (Camb).* **2007**, *0* (27), 2853–2854.
(77) Gartzia-Rivero, L.; Bañuelos, J.; López-Arbeloa, I. Photoactive Nanomaterials Inspired by Nature: LTL Zeolite Doped with Laser Dyes as Artificial Light Harvesting Systems. *Materials (Basel).* **2017**, *10* (5), 495.
(78) Gigli, L.; Arletti, R.; Tabacchi, G.; Fois, E.; Vitillo, J. G.; Martra, G.; Agostini, G.; Quartieri, S.; Vezzalini, G. Close-Packed Dye Molecules in Zeolite Channels Self-Assemble into Supramolecular Nanoladders. *J. Phys. Chem. C* **2014**, *118* (29), 15732–15743.
(79) Gigli, L.; Arletti, R.; Tabacchi, G.; Fabbiani, M.; Vitillo, J. G.; Martra, G.; Devaux, A.; Miletto, I.; Quartieri, S.; Calzaferri, G.; et al. Structure and Host–Guest Interactions of Perylene–Diimide Dyes in Zeolite L Nanochannels. *J. Phys. Chem. C* **2018**, *122* (6), 3401–3418.
(80) Vohra, V.; Calzaferri, G.; Destri, S.; Pasini, M.; Porzio, W.; Botta, C. Toward White Light Emission through Efficient Two-Step Energy Transfer in Hybrid

Nanofibers. *ACS Nano* **2010**, *4* (3), 1409–1416.
(81) Wang, Y.; Li, H. Luminescent Materials of Zeolite Functionalized with Lanthanides. *CrystEngComm* **2014**, *16* (42), 9764–9778.
(82) Sola-Llano, R.; Fujita, Y.; Gómez-Hortigüela, L.; Alfayate, A.; Ujii, H.; Fron, E.; Toyouchi, S.; Perez-Pariente, J.; Lopez-Arbeloa, I.; Martinez-Martinez, V. One-Directional Antenna Systems: Energy Transfer from Monomers to J-Aggregates within 1D Nanoporous Aluminophosphates. *ACS Photonics* **2018**, *5* (1), 151–157.
(83) Popović, Z.; Otter, M.; Calzaferri, G.; De Cola, L. Self-Assembling Living Systems with Functional Nanomaterials. *Angew. Chemie Int. Ed.* **2007**, *46* (32), 6188–6191.
(84) Kehr, N. S. Microcontact Printing of (Bio)Molecules on Self-Assembled Monolayers of Zeolites L and Surface Mediated Drug Delivery. *Adv. Porous Mater.* **2018**, *6* (1), 19–27.
(85) Lülf, H.; Bertucci, A.; Septiadi, D.; Corradini, R.; De Cola, L. Multifunctional Inorganic Nanocontainers for DNA and Drug Delivery into Living Cells. *Chem. - A Eur. J.* **2014**, *20* (35), 10900–10904.
(86) Wang, Y.; Li, H.; Feng, Y.; Zhang, H.; Calzaferri, G.; Ren, T. Orienting Zeolite L Microcrystals with a Functional Linker. *Angew. Chemie - Int. Ed.* **2010**, *49* (8), 1434–1438.
(87) Calzaferri, G.; Méallet-Renault, R.; Brühwiler, D.; Pansu, R.; Dolamic, I.; Dienel, T.; Adler, P.; Li, H.; Kunzmann, A. Designing Dye-Nanochannel Antenna Hybrid Materials for Light Harvesting, Transport and Trapping. *ChemPhysChem* **2011**, *12* (3), 580–594.
(88) Doungmanee, S.; Siritanon, T.; Insuwan, W.; Jungsuttiwong, S.; Rangsriwatananon, K. Multi Step Energy Transfer between Three Si_LTL and SiGe_LTL Zeolite-Loaded Dyes. *J. Porous Mater.* **2018**, *25* (5), 1381–1389.
(89) Schulz-Ekloff, G.; Wöhrle, D.; van Duffel, B.; Schoonheydt, R. A. Chromophores in Porous Silicas and Minerals: Preparation and Optical Properties. *Microporous Mesoporous Mater.* **2002**, *51* (2), 91–138.
(90) Van Speybroeck, V.; Hemelsoet, K.; Joos, L.; Waroquier, M.; Bell, R. G.; Catlow, C. R. A. Advances in Theory and Their Application within the Field of Zeolite Chemistry. *Chem. Soc. Rev.* **2015**, *44* (20), 7044–7111.
(91) Paul, G.; Bisio, C.; Braschi, I.; Cossi, M.; Gatti, G.; Gianotti, E.; Marchese, L. Combined Solid-State NMR, FT-IR and Computational Studies on Layered and Porous Materials. *Chem. Soc. Rev.* **2018**, *47* (15), 5684–5739.
(92) Demontis, P.; Suffritti, G. B.; Quartieri, S.; Gamba, A.; Fois, E. S. Molecular Dynamics Studies on Zeolites. Part 5.—Discussion of the Structural Changes of Silicalite. *J. Chem. Soc., Faraday Trans.* **1991**, *87* (10), 1657–1663.
(93) Pintus, A. M.; Gabrieli, A.; Pazzona, F. G.; Pireddu, G.; Demontis, P. *Molecular QCA Embedding in Microporous Materials*; 2018.
(94) Rimola, A.; Costa, D.; Sodupe, M.; Lambert, J.-F.; Ugliengo, P. Silica Surface Features and Their Role in the Adsorption of Biomolecules: Computational Modeling and Experiments. *Chem. Rev.* **2013**, *113* (6), 4216–4313.
(95) Fois, E.; Gamba, A.; Tabacchi, G. Influence of Silanols Condensation on Surface Properties of Micelle-Templated Silicas: A Modelling Study. *Microporous Mesoporous Mater.* **2008**, *116* (1–3), 718–722.
(96) Fois, E.; Gamba, A.; Tabacchi, G.; Coluccia, S.; Martra, G. Ab Initio Study of Defect Sites at the Inner Surfaces of

Mesoporous Silicas. *J. Phys. Chem. B* **2003**, *107* (39), 10767–10772.
(97) Coudert, F. X.; Fuchs, A. H. Computational Characterization and Prediction of Metal-Organic Framework Properties. *Coord. Chem. Rev.* **2015**, *307*, 211–236.
(98) Fischer, M.; Gomes, J. R. B.; Jorge, M. Computational Approaches to Study Adsorption in MOFs with Unsaturated Metal Sites. *Mol. Simul.* **2014**, *40* (7–9), 537–556.
(99) Fraux, G.; Coudert, F.-X. Recent Advances in the Computational Chemistry of Soft Porous Crystals. *Chem. Commun.* **2017**, *53* (53), 7211–7221.
(100) Bussemer, B.; Munsel, D.; Wünscher, H.; Mohr, G. J.; Grummt, U. W. Electronic Properties of Neutral Dyes in the Channels of Zeolite L: A Combined Spectroscopic and Quantum Chemical Study. *J. Phys. Chem. B* **2007**, *111* (1), 8–15.
(101) Fois, E.; Tabacchi, G.; Calzaferri, G. Interactions, Behavior, and Stability of Fluorenone inside Zeolite Nanochannels. *J. Phys. Chem. C* **2010**, *114* (23), 10572–10579.
(102) Zhou, X.; Wesolowski, T. A.; Tabacchi, G.; Fois, E.; Calzaferri, G.; Devaux, A. First-Principles Simulation of the Absorption Bands of Fluorenone in Zeolite L. *Phys. Chem. Chem. Phys.* **2013**, *15* (1), 159–167.
(103) Insuwan, W.; Rangsriwatananon, K.; Meeprasert, J.; Namuangruk, S.; Surakhot, Y.; Kungwan, N.; Jungsuttiwong, S. Combined Experimental and Theoretical Investigation on Photophysical Properties of Trans-Azobenzene Confined in LTL Zeolite: Effect of Cis-Isomer Forming. *Microporous Mesoporous Mater.* **2014**, *197*, 348–357.
(104) Insuwan, W.; Rangsriwatananon, K.; Meeprasert, J.; Namuangruk, S.; Surakhot, Y.; Kungwan, N.; Jungsuttiwong, S. Combined Experimental and Theoretical Investigation on Fluorescence Resonance Energy Transfer of Dye Loaded on LTL Zeolite. *Microporous Mesoporous Mater.* **2017**, *241*, 372–382.
(105) Fois, E.; Tabacchi, G.; Calzaferri, G. Orientation and Order of Xanthene Dyes in the One-Dimensional Channels of Zeolite L: Bridging the Gap between Experimental Data and Molecular Behavior. *J. Phys. Chem. C* **2012**, *116* (31), 16784–16799.
(106) Viani, L.; Minoia, A.; Cornil, J.; Beljonne, D.; Egelhaaf, H. J.; Gierschner, J. Resonant Energy Transport in Dye-Filled Monolithic Crystals of Zeolite L: Modeling of Inhomogeneity. *J. Phys. Chem. C* **2016**, *120* (48), 27192–27199.
(107) Cucinotta, F.; Guenet, A.; Bizzarri, C.; Mroz, W.; Botta, C.; Milian-Medina, B.; Gierschner, J.; De Cola, L. Energy Transfer at the Zeolite l Boundaries: Towards Photo- and Electroresponsive Materials. *Chempluschem* **2014**, *79* (1), 45–57.
(108) Calzaferri, G. Entropy in Multiple Equilibria, Theory and Applications. *Phys. Chem. Chem. Phys.* **2017**, *19* (16), 10611–10621.
(109) Tabacchi, G.; Fois, E.; Calzaferri, G. Structure of Nanochannel Entrances in Stopcock-Functionalized Zeolite L Composites. *Angew. Chemie Int. Ed.* **2015**, *54* (38), 11112–11116.
(110) Tabacchi, G.; Calzaferri, G.; Fois, E. One-Dimensional Self-Assembly of Perylene-Diimide Dyes by Unidirectional Transit of Zeolite Channel Openings. *Chem. Commun.* **2016**, *52* (75), 11195–11198.
(111) Gigli, L.; Arletti, R.; Fois, E.; Tabacchi, G.; Quartieri, S.; Dmitriev, V.; Vezzalini, G. Unravelling the High-

Pressure Behaviour of Dye-Zeolite L Hybrid Materials. *Crystals* **2018**, *8* (2), 79.
(112) Sun, L.; Xing, H.; Liang, Z.; Yu, J.; Xu, R. A 4 + 4 Strategy for Synthesis of Zeolitic Metal-Organic Frameworks: An Indium-MOF with SOD Topology as a Light-Harvesting Antenna. *Chem. Commun.* **2013**, *49* (95), 11155–11157.
(113) Chen, F.; Wang, L.; Xing, Y.; Zhang, J. Stable Photoluminescence of Lanthanide Complexes in Aqueous Media through Metal-Organic Frameworks Nanoparticles with Plugged Surface. *J. Colloid Interface Sci.* **2018**, *527*, 68–77.
(114) Kim, J. G.; Noh, T. H.; Cho, Y.; Park, J. K.; Jung, O.-S. A Triple-Function Nanotube as a Reactant Reservoir, Reaction Platform, and Byproduct Scavenger for Photo-Cyclopropanation. *Chem. Commun.* **2016**, *52* (12), 2545–2548.
(115) Noh, T. H.; Jang, J.; Hong, W.; Lee, H.; Jung, O.-S. Truncated Trigonal Prismatic Tubular Crystals Consisting of a Zeolite L-Mimic Metal-Organic Framework. *Chem. Commun.* **2014**, *50* (56), 7451–7454.
(116) Gigli, L.; Arletti, R.; Quartieri, S.; Di Renzo, F.; Vezzalini, G. The High Thermal Stability of the Synthetic Zeolite K–L: Dehydration Mechanism by in Situ SR-XRPD Experiments. *Microporous Mesoporous Mater.* **2013**, *177*, 8–16.
(117) Barrer, R. M. *Hydrothermal Chemistry of Zeolites*; Academic Press: London ; UK., 1982.
(118) Gigli, L.; Vezzalini, G.; Quartieri, S.; Arletti, R. Compressibility Behavior and Pressure-Induced over-Hydration of Zeolite K–AlSi-L. *Microporous Mesoporous Mater.* **2019**, *276*, 160–166.
(119) Comboni, D.; Gatta, G. D.; Lotti, P.; Merlini, M.; Hanfland, M. Crystal-Fluid Interactions in Laumontite. *Microporous Mesoporous Mater.* **2018**, *263*, 86–95.
(120) Likhacheva, A. Y.; Seryotkin, Y. V.; Manakov, A. Y.; Goryainov, S. V.; Ancharov, A. I.; Sheromov, M. A. Pressure-Induced over-Hydration of Thomsonite: A Synchrotron Powder Diffraction Study. *Am. Mineral.* **2007**, *92* (10), 1610–1615.
(121) Devaux, A.; Minkowski, C.; Calzaferri, G. Electronic and Vibrational Properties of Fluorenone in the Channels of Zeolite L. *Chem. - A Eur. J.* **2004**, *10* (10), 2391–2408.
(122) Barrer, R. M.; Villiger, H. The Crystal Structure of the Synthetic Zeolite L. *Zeitschrift für Krist. - Cryst. Mater.* **1969**, *128* (1–6), 352–370.
(123) Artioli, G.; Kvick, A. Synchrotron X-Ray Rietveld Study of Perlialite, the Natural Counterpart of Synthetic Zeolite-L. *Eur. J. Mineral.* **1990**, *2* (6), 749–760.
(124) Lee, Y.; Kim, S. J.; Ahn, D. C.; Shin, N. S. Confined Water Clusters in a Synthetic Rubidium Gallosilicate with Zeolite LTL Topology. *Chem. Mater.* **2007**, *19* (9), 2277–2282.
(125) Depmeier, W. Some Examples of Temperature and Time Resolved Studies of the Dehydration and Hydration Behavior of Zeolites and Clathrates. *Part. Part. Syst. Charact.* **2009**, *26* (3), 138–150.
(126) Hu, X.; Depmeier, W. Pitfalls in the X-Ray Structure Determination of Pseudosymmetric Sodalites, and Possibly Zeolites. *Zeitschrift fur Krist. - New Cryst. Struct.* **1992**, *201* (1–2), 99–111.
(127) Perdew, J. P.; Burke, K.; Ernzerhof, M. Generalized Gradient Approximation Made Simple. *Phys. Rev. Lett.* **1996**, *77* (18), 3865–3868.
(128) Grimme, S. Semiempirical GGA-Type Density Functional Constructed with a Long-Range Dispersion Correction. *J. Comput. Chem.* **2006**, *27* (15), 1787–1799.

(129) Kremleva, A.; Vogt, T.; Rösch, N. Monovalent Cation-Exchanged Natrolites and Their Behavior under Pressure. A Computational Study. *J. Phys. Chem. C* **2013**, *117* (37), 19020–19030.
(130) Fischer, M. Template Effects on the Pressure-Dependent Behavior of Chabazite-Type Fluoroaluminophosphates: A Computational Approach. *Phys. Chem. Miner.* **2018**, 1–17.
(131) Gatta, G. D.; Tabacchi, G.; Fois, E.; Lee, Y. Behaviour at High Pressure of Rb7NaGa8Si12O40·3H2O (a Zeolite with EDI Topology): A Combined Experimental–computational Study. *Phys. Chem. Miner.* **2016**, *43* (3), 209–216.
(132) Fischer, M.; Bell, R. G. Modeling CO_2 Adsorption in Zeolites Using DFT-Derived Charges: Comparing System-Specific and Generic Models. *J. Phys. Chem. C* **2013**, *117* (46), 24446–24454.
(133) Fischer, M.; Bell, R. G. Interaction of Hydrogen and Carbon Dioxide with Sod-Type Zeolitic Imidazolate Frameworks: A Periodic DFT-D Study. *CrystEngComm* **2014**, *16* (10), 1934.
(134) Li, G.; Pidko, E. A. The Nature and Catalytic Function of Cation Sites in Zeolites: A Computational Perspective The Nature and Catalytic Function of Cation Sites in Zeolites: A Computational Perspective. *ChemCatChem* **2018**.
(135) Spanó, E.; Tabacchi, G.; Gamba, A.; Fois, E. On the Role of Ti(IV) as a Lewis Acid in the Chemistry of Titanium Zeolites: Formation, Structure, Reactivity, and Aging of Ti-Peroxo Oxidizing Intermediates. A First Principles Study. *J. Phys. Chem. B* **2006**, *110* (43), 21651–21661.
(136) Valenzano, L.; Civalleri, B.; Chavan, S.; Palomino, G. T.; Areán, C. O.; Bordiga, S. Computational and Experimental Studies on the Adsorption of CO, N 2 , and CO 2 on Mg-MOF-74. *J. Phys. Chem. C* **2010**, *114* (25), 11185–11191.
(137) Fischer, M. Structure and Bonding of Water Molecules in Zeolite Hosts: Benchmarking Plane-Wave DFT against Crystal Structure Data. *Zeitschrift für Krist. - Cryst. Mater.* **2015**, *230* (5), 325–336.
(138) Fischer, M.; Angel, R. J. Accurate Structures and Energetics of Neutral-Framework Zeotypes from Dispersion-Corrected DFT Calculations. *J. Chem. Phys.* **2017**, *146* (17), 174111.
(139) Hay, H.; Ferlat, G.; Casula, M.; Seitsonen, A. P.; Mauri, F. Dispersion Effects in SiO 2 Polymorphs: An Ab Initio Study. *Phys. Rev. B* **2015**, *92*, 144111.
(140) Fischer, M.; Evers, F. O.; Formalik, F.; Olejniczak, A. Benchmarking DFT-GGA Calculations for the Structure Optimisation of Neutral-Framework Zeotypes. *Theor. Chem. Acc.* **2016**, *135* (12), 257.
(141) Fischer, M.; Delgado, M. R.; Areán, C. O.; Duran, C. O. CO Adsorption Complexes in Zeolites: How Does the Inclusion of Dispersion Interactions Affect Predictions Made from DFT Calculations? The Case of Na-CHA. *Theor. Chem. Acc.* **2015**, *134* (7), 91.
(142) Arletti, R.; Fois, E.; Tabacchi, G.; Quartieri, S.; Vezzalini, G. Pressure-Induced Penetration of Water-Ethanol Mixtures in All-Silica Ferrierite. *Adv. Sci. Lett.* **2017**, *23* (6), 5966–5969.
(143) Giannozzi, P.; Andreussi, O.; Brumme, T.; Bunau, O.; Buongiorno Nardelli, M.; Calandra, M.; Car, R.; Cavazzoni, C.; Ceresoli, D.; Cococcioni, M.; et al. Advanced Capabilities for Materials Modelling with Quantum ESPRESSO. *J. Phys. Condens. Matter* **2017**, *29* (46), 465901.
(144) IBM Corp. 1990–2017; MPI für Festkörperforschung

Stuttgart 1997–2001. CPMD: Car Parrinello Molecular Dynamics. 2017.
(145) Vanderbilt, D. Soft Self-Consistent Pseudopotentials in a Generalized Eigenvalue Formalism. *Phys. Rev. B* **1990**, *41* (11), 7892–7895.
(146) Troullier, N.; Martins, J. L. Efficient Pseudopotentials for Plane-Wave Calculations. *Phys. Rev. B* **1991**, *43* (3), 1993–2006.
(147) Kleinman, L.; Bylander, D. M. Efficacious Form for Model Pseudopotentials. *Phys. Rev. Lett.* **1982**, *48* (20), 1425–1428.
(148) Fois, E.; Tabacchi, G.; Barreca, D.; Gasparotto, A.; Tondello, E. “Hot” Surface Activation of Molecular Complexes: Insight from Modeling Studies. *Angew. Chemie - Int. Ed.* **2010**, *49* (11), 1944–1948.
(149) Tabacchi, G.; Fois, E.; Barreca, D.; Gasparotto, A. CVD Precursors for Transition Metal Oxide Nanostructures: Molecular Properties, Surface Behavior and Temperature Effects. *Phys. status solidi* **2014**, *211* (2), 251–259.
(150) Tabacchi, G.; Gianotti, E.; Fois, E.; Martra, G.; Marchese, L.; Coluccia, S.; Gamba, A. Understanding the Vibrational and Electronic Features of Ti(IV) Sites in Mesoporous Silicas by Integrated Ab Initio and Spectroscopic Investigations. *J. Phys. Chem. C* **2007**, *111* (13), 4946–4955.
(151) Tilocca, A.; Fois, E. The Color and Stability of Maya Blue: TDDFT Calculations. *J. Phys. Chem. C* **2009**, *113* (20), 8683–8687.
(152) Barreca, D.; Fois, E.; Gasparotto, A.; Seraglia, R.; Tondello, E.; Tabacchi, G. How Does CuII Convert into CuI? An Unexpected Ring-Mediated Single-Electron Reduction. *Chem. - A Eur. J.* **2011**, *17* (39), 10864–10870.
(153) Deiana, C.; Fois, E.; Martra, G.; Narbey, S.; Pellegrino, F.; Tabacchi, G. On the Simple Complexity of Carbon Monoxide on Oxide Surfaces: Facet-Specific Donation and Backdonation Effects Revealed on TiO2 Anatase Nanoparticles. *ChemPhysChem* **2016**, *17* (13), 1956–1960.
(154) Fischer, M. DFT-Based Evaluation of Porous Metal Formates for the Storage and Separation of Small Molecules. *Microporous Mesoporous Mater.* **2016**, *219*, 249–257.
(155) Formalik, F.; Fischer, M.; Rogacka, J.; Firlej, L.; Kuchta, B. Effect of Low Frequency Phonons on Structural Properties of ZIFs with SOD Topology. *Microporous Mesoporous Mater.* **2018**.
(156) Formalik, F.; Fischer, M.; Rogacka, J.; Firlej, L.; Kuchta, B. Benchmarking of GGA Density Functionals for Modeling Structures of Nanoporous, Rigid and Flexible MOFs. *J. Chem. Phys.* **2018**, *149* (6), 064110.
(157) Tabacchi, G.; Fois, E.; Barreca, D.; Gasparotto, A. Opening the Pandora’s Jar of Molecule-to-Material Conversion in Chemical Vapor Deposition: Insights from Theory. *Int. J. Quantum Chem.* **2014**, *114* (1), 1–7.
(158) Fois, E. S.; Penman, J. I.; Madden, P. A. Self-interaction Corrected Density Functionals and the Structure of Metal Clusters. *J. Chem. Phys.* **1993**, *98* (8), 6352–6360.
(159) Dudarev, S.; Botton, G. Electron-Energy-Loss Spectra and the Structural Stability of Nickel Oxide: An LSDA+U Study. *Phys. Rev. B - Condens. Matter Mater. Phys.* **1998**, *57* (3), 1505–1509.
(160) Himmetoglu, B.; Floris, A.; de Gironcoli, S.; Cococcioni, M. Hubbard-Corrected DFT Energy Functionals: The LDA+U Description of Correlated Systems. *Int. J. Quantum Chem.* **2014**, *114* (1), 14–49.
(161) Lee, K.; Howe, J. D.; Lin, L. C.; Smit, B.; Neaton, J. B.

Small-Molecule Adsorption in Open-Site Metal-Organic Frameworks: A Systematic Density Functional Theory Study for Rational Design. *Chem. Mater.* **2015**, *27* (3), 668–678.
(162) Trudu, F.; Tabacchi, G.; Gamba, A.; Fois, E. Water in Acid Boralites: Hydration Effects on Framework B Sites. *J. Phys. Chem. C* **2008**, *112* (39), 15394–15401.
(163) Trudu, F.; Tabacchi, G.; Gamba, A.; Fois, E. First Principles Studies on Boron Sites in Zeolites. *J. Phys. Chem. A* **2007**, *111* (45), 11626–11637.
(164) Demontis, P.; Gulín-González, J.; Masia, M.; Suffritti, G. B. The Behaviour of Water Confined in Zeolites: Molecular Dynamics Simulations versus Experiment. *J. Phys. Condens. Matter* **2010**, *22* (28), 284106.
(165) Hellström, M.; Ceriotti, M.; Behler, J. Nuclear Quantum Effects in Sodium Hydroxide Solutions from Neural Network Molecular Dynamics Simulations. *J. Phys. Chem. B* **2018**, *122* (44), 10158–10171.
(166) Tuckerman, M. E.; Marx, D.; Parrinello, M. The Nature and Transport Mechanism of Hydrated Hydroxide Ions in Aqueous Solution. *Nature* **2002**, *417* (6892), 925–929.
(167) Chen, B.; Park, J. M.; Ivanov, I.; Tabacchi, G.; Klein, M. L.; Parrinello, M. First-Principles Study of Aqueous Hydroxide Solutions. *J. Am. Chem. Soc.* **2002**, *124* (29), 8534–8535.
(168) Fois, E.; Gamba, A.; Tabacchi, G. Structure and Dynamics of a Brønsted Acid Site in a Zeolite: An Ab Initio Study of Hydrogen Sodalite. *J. Phys. Chem. B* **1998**, *102* (20), 3974–3979.
(169) Muñoz-Santiburcio, D.; Marx, D. Chemistry in Nanoconfined Water. *Chem. Sci.* **2017**, *8* (5), 3444–3452.
(170) Fois, E.; Gamba, A.; Medici, C.; Tabacchi, G. Intermolecular Electronic Excitation Transfer in a Confined Space: A First-Principles Study. *ChemPhysChem* **2005**, *6* (9), 1917–1922.
(171) Köfinger, J.; Hummer, G.; Dellago, C. Single-File Water in Nanopores. *Phys. Chem. Chem. Phys.* **2011**, *13* (34), 15403.
(172) Devaux, A.; Calzaferri, G.; Belser, P.; Cao, P.; Brühwiler, D.; Kunzmann, A. Efficient and Robust Host-Guest Antenna Composite for Light Harvesting. *Chem. Mater.* **2014**, *26* (23), 6878–6885.